Design of Longitudinal Control System for Brushless Motor Electric Vehicle Using VSTC Control Theory*

Duong-Phuoc-AN**, Kikuo NEZU**
and Tsuneo AKUTO***

This paper is concerned with the design of a slide mode control system from the view point of practical application. The problem is treated using the asymptotic reaching law method for assuring global stabilization, and the chattering phenomenon is alleviated by the saturated function of the boundary layer. The design algorithm is simple and applicable to a nonlinear system including disturbances and uncertainties with high robustness. Its effectiveness is proven by simulation as well as a bench experiment of a brushless motor vehicle.

Key Words: Slide Mode, Chattering, Saturated Function, Boundary Layer, Nonlinear Control, Brushless Motor, Electric Vehicle

1. Introduction

In longitudinal control of an electric vehicle, mechanical dynamics such as rolling friction and slip between the tire and road surface, air resistance, and efficiency of reduction gear are important factors. In particular, rolling friction is related to the slip ratio, and in high-velocity operation, air resistance is proportional to speed; these are important elements that are must be considered. Also, because the driving system consists of a brushless motor and inverter, it is an electrical control system. In general, a longitudinal control system can be thought of as a nonlinear electromechanical control system. In this case, in considering the uncertainty of modeling system, the variation of parameters and the influence of disturbance, a strong robust control logic such as VSTC is thought to be effective. By applying this control logic to the electric vehicle, we can obtain high stabilization, dynamic response and desirable tracking control with respect to command velocity.

In this paper, we introduce an optimal tracking longitudinal control system of an electric vehicle by using the superior characteristics of VSTC control logic for performing an antispin in acceleration, and antiskid in deceleration. As a result, we can improve the running stability and achieve a comfortable ride.

However, in VSTC control, the chattering phenomenon occurs, which poses a major difficulty. In this paper, we propose a saturated function which is simple but effective for alleviating chatter. The effectiveness of the control logic is proven by simulation and a bench experiment.

Nomenclature

V : Velocity of car body (m/s)
$\dot{V}$: Acceleration • deceleration (m/s^2)
ω : Angular velocity of wheel (Rad/s)
$\dot{\omega}$: Angular acceleration of wheel (Rad/s^2)
W, M : Total weight (N), mass (kg) of vehicle body
g : Acceleration of gravity (m/s^2)

* Received 26th January, 1995. Japanese original: Trans. Jpn. Soc. Mech. Eng., Vol. 60, No. 574, C (1994), pp. 2036-2044. (Received 13th October, 1993)
** Faculty of Engineering, Gunma University, 1-5-1 Tenjin-cho, Kiryu 376, Japan
*** Mitsuba Denki Mfg. Co., Ltd., 1-2681 Hirosawa-cho, Kiryu 376, Japan

l, h : Wheel base (m), height of center of gravity (m)
H : Height of point of application of concentrated force equivalent to air resistance (m)
T : Driving torque for tire and rotary components (N•m)
T_B : Breaking torque (N•m)
K_B : Breaking coefficient (N•m/V)
C_d : Air resistance coefficient
ρ : Air density (kg/m^3)
A : Front projected area of vehicle body (m^2)
r_w : Wheel effective radius(m)
I, J : Inertial moment (kg•m^2)
i : Reduction gear ratio
η : Transmission efficiency
W_L : Disturbance (N)
B_w : Viscous friction coefficient (N•m•s^2/Rad^2)
μ, λ : Friction coefficient, slip ratio ; $\mu=f(\lambda)$
K_t : Torque constant (N•m/A)
K_e : Induction voltage constant (V•s/Rad)
T_e : Driving torque on motor shaft (N•m)
u_m, u_B : Motor, brake control input (V)
K, R_a : Control gain, coil resistance (Ω)
L : Coil inductance (H)

2. Mathematical Model of an Electric Vehicle

We discuss the longitudinal control of electric vehicles during acceleration and deceleration.

2.1 The case of acceleration

The running state is shown in Fig. 1, and the model of the driving system is shown in Fig. 2. Also, the dynamics between the road and vehicle body and wheel are shown in Fig. 3. We consider the case where the vehicle has rear-wheel drive. Because the front tires are passive, their circumferential velocities are equal to vehicle body velocity. This means that the rolling friction coefficient upon the front wheels is very smaller, and can be ignored, i. e., $\mu_f \approx 0$.

The driving force of the vehicle is generated by rolling friction on rear wheel. The resistances consist of inertial force and air resistance and are given by

$$\frac{W}{g}\dot{V}=\mu_r W_r-\frac{1}{2}\rho C_d A V^2-W_L \qquad (1)$$

where W_r and W_f are the loads on rear wheels and front wheels, respectively

$$W_r=\frac{Wl_f}{l}+\frac{Wh}{lg}\dot{V}+\frac{\rho C_d A H}{2l}V^2 \qquad (2.a)$$

$$W_f=\frac{Wl_r}{l}-\frac{Wh}{lg}\dot{V}-\frac{\rho C_d A H}{2l}V^2 \qquad (2.b)$$

From Eqs. (1) and (2.a), we get

$$\dot{V}=-\frac{g\rho C_d A(l-\mu_r H)}{2W(l-\mu_r h)}V^2+\frac{\mu_r g l_f}{(l-\mu_r h)}-\frac{gl}{W(l-\mu_r h)}W_L \qquad (3)$$

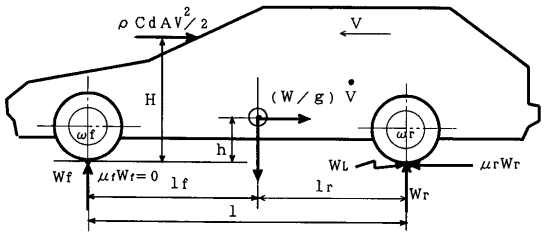

Fig. 1 State of electric vehicle in acceleration and constant velocity periods

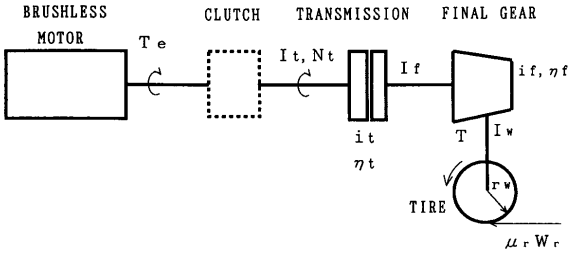

Fig. 2 Driving system

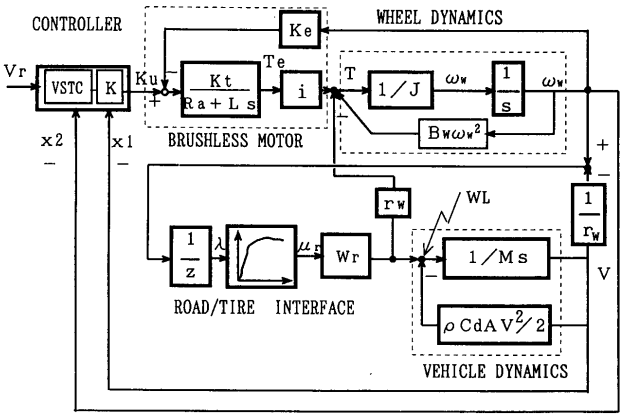

Fig. 3 Diagram of driving dynamics of electric vehicle

In the same manner as above, we consider the rear wheel shown in Fig. 3, and obtain

$$J\dot{\omega}_w=T-\mu_r W_r r_w-B_w\omega_w^2-W_L r_w \qquad (4)$$

Using W_r of Eq. (2.a),

$$\dot{\omega}_w=-\frac{B_w}{J}\omega_w^2-\frac{\mu_r r_w W l_f}{Jl}-\frac{\mu_r r_w W h}{Jlg}\dot{V}-\frac{\mu_r r_w \rho C_d A H}{2Jl}V^2+\frac{T}{J}-\frac{W_L r_w}{J} \qquad (5)$$

J is inertial moment of rotary elements such as the motor, wheels, driving transmission system and is driving shaft, and is expressed by

$$J=I_w+\{I_f+(I_t+I_e)\eta_t i_t^2\}\eta_f i_f^2 \qquad (6)$$

T is the driving torque of the wheel. In the case of using a "3-phase, 4-poles" brushless motor, T is calculated by[1]

$$T=\frac{3K_t\eta i(Ku_m-K_\theta\omega_w)}{R_a+Ls} \qquad (7)$$

By substituting T of Eq. (7) into Eq. (5), and rearranging, the following is obtained.

$$\dot{\omega}_w=-\frac{B_w}{J}\omega_w^2-\frac{3K_t\eta iK_e}{J(R_a+Ls)}\omega_w-\frac{\mu_r r_w Wl_f}{Jl}-\frac{\mu_r r_w Wh}{Jlg}\dot{V}-\frac{\mu_r r_w\rho C_d AH}{2Jl}V^2+\frac{3KK_t\eta i}{J(R_a+Ls)}u_m-\frac{W_L r_w}{J} \quad (8)$$

Friction coefficient μ is dependent on slip ratio. Figure 4 shows the relationship between μ and slip ratio λ[2),3)].

$$\mu=f(\lambda) \quad (9)$$

$$\lambda=\frac{\omega_w-V/r_w}{z};\begin{cases}z=\omega_w & \text{(for acceleration)}\\ z=V/r_w & \text{(for deceleration)}\end{cases} \quad (10)$$

By substituting $\dot{V}$ of Eq. (3) into Eq. (8), and replacing angular velocity of wheel ω_w with x_2 and equivalent angular velocity of vehicle body V/r_w with x_1, the state equation of the driving system is arranged as

$$\dot{x}_1=-\frac{g\rho C_d Ar_w(l-\mu_r H)}{2W(l-\mu_r h)}x_1^2+\frac{\mu_r gl_f}{r_w(l-\mu_r h)}-\frac{gl}{r_w W(l-\mu_r h)}W_L \quad (11)$$

$$\dot{x}_2=-\frac{B_w}{J}x_2^2-\frac{3K_tK_e\eta i}{J(R_a+Ls)}x_2-\frac{\mu_r r_w^2\rho C_d A(H-h)}{2J(l-\mu_r h)}x_1^2-\frac{\mu_r r_w Wl_f}{J(l-\mu_r h)}+\frac{3KK_t\eta i}{J(R_a+Ls)}u_m-\frac{r_w lW_L}{J(l-\mu_r h)} \quad (12)$$

Setting $x=[x_1\ x_2]^T$ as the state vector, $u=[0\ u_m]^T$ as control input and $w=W_L$ as disturbance, we get the state equation

$$\dot{x}=F(x)+Gu+Dw$$
$$y=x \quad (13)$$

where F is state matrix, G is nonsingular control matrix and D is external disturbance matrix, expressed by the following equations.

$$F=\begin{bmatrix}-\frac{g\rho C_d Ar_w(l-\mu_r H)}{2W(l-\mu_r h)}x_1^2+\frac{\mu_r gl_f}{r_w(l-\mu_r h)}\\ \left\{-\frac{\mu_r r_w^3\rho C_d A(H-h)}{2J(l-\mu_r h)}x_1^2-\frac{B_w}{J}x_2^2-\frac{3K_tK_e\eta i}{J(R_a+Ls)}x_2-\frac{\mu_r r_w Wl_f}{J(l-\mu_r h)}\right\}\end{bmatrix}$$

$$G=\begin{bmatrix}\alpha & 0\\ 0 & \frac{3KK_t\eta i}{J(R_a+Ls)}\end{bmatrix};\ D=\begin{bmatrix}\frac{-gl}{r_w W(l-\mu_r h)}\\ \frac{-r_w l}{J(l-\mu_r h)}\end{bmatrix} \quad (14)$$

α is an arbitrary constant which is defined such that G may become a nonsingular matrix.

2.2 The case of deceleration

In the case of deceleration, the braking force distributed between front and rear wheels has an effect on running performances such as breaking distance, stability of vehicle body and direction control of vehicle. In ideal braking deceleration, the rolling friction coefficients of front and rear tires against the road surface are equal[3].

In this paper, it is assumed that both the front and rear wheels follow a reference deceleration velocity at the same time. Running state and dynamics diagrams of the vehicle are shown in Fig. 5 and Fig. 6,

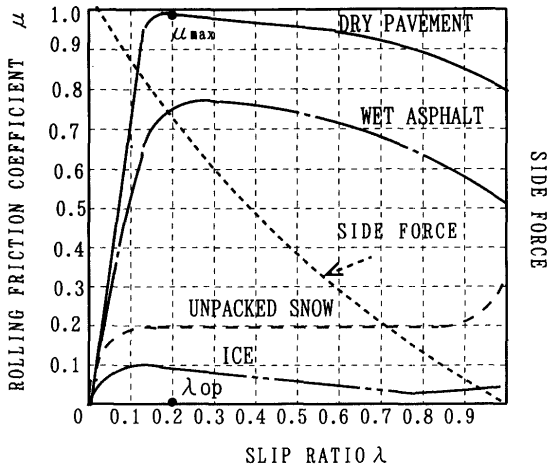

Fig. 4 The relationship between slip ratio and rolling friction coefficient (Side force is shown only qualitatively)

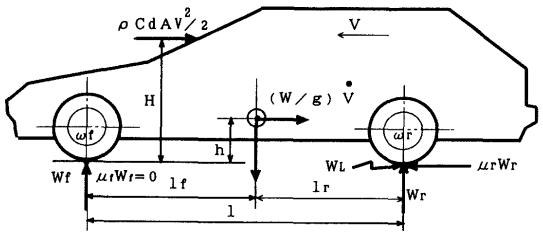

Fig. 5 Braking state of an electric vehicle

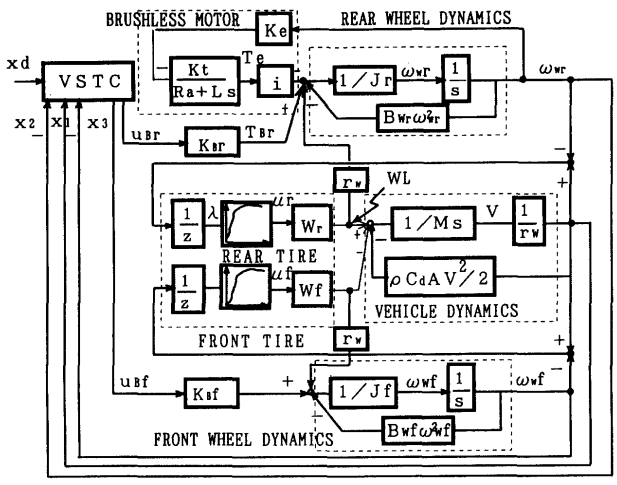

Fig. 6 Diagrams of braking dynamics of electric vehicle

respectively.

In deceleration, the load W_r on rear wheels is less than that in the case of acceleration and the load W_f on front wheels increases. This phenomenon is called load shift. As shown in Fig. 4, the friction coefficient becomes maximum when the slip ratio is 10%-20%. At the same time, the side force of the tire is maximum when the slip ratio is 0, linearly decreases as the slip ratio increases, and becomes 0 when the slip ratio is 100% in the so-called all-locked state. On the friction-slip curve, a positive slope indicates stable braking, whereas a negative slope indicates unstable braking. On considering the characteristics of friction coefficients and slip, it is necessary to control the rotation of tires so that slip ratio is about 10%-20% where side force is sufficiently strong and rolling friction coefficient becomes maximum, and to give the maximal braking force and shortest stable braking distance without wheel locking. Consequently, both front and rear wheels must be controlled to track the reference velocity of the vehicle body so that 20 % slip ratio is maintained. Velocity satisfies the conditions that the vehicle body experiences during stable braking (i.e., $\mu_r=\mu_f$) and stops in the shortest distance ($\lambda=\lambda_{op}$, $\mu=\mu_{\max}$), we get

$$\frac{W}{g}\dot{V}_{op}=\mu_{\max}W-\frac{1}{2}\rho C_d V_{op}^2-W_L\ ;\ \mu_{\max}<0 \tag{15.a}$$

$$V_{op}=aTan(-bt+\mathrm{Tan}^{-1}\,c) \tag{15.b}$$

$$a=\sqrt{\frac{2(-\mu_{\max}W+W_L)}{\rho C_d A}},\ b=\frac{g}{W}\sqrt{\frac{\rho C_d A(-\mu_{\max}W+W_L)}{2}},\ c=V_0\sqrt{\frac{\rho C_d A}{2(-\mu_{\max}W+W_L)}}\ ;\ W_L>\mu_{\max}W \tag{15.c}$$

where V_0 is the initial velocity in deceleration. It should also be stressed that in braking, $\mu_{\max}<0$. By controlling vehicle body velocity to track optimal velocity V_{op}, and both front and rear wheels to track $(1-\lambda_{op})\times V_{op}/r_w$, these dynamic equations can rewritten as

$$\frac{W}{g}\dot{V}=\mu_r W_r+\mu_f W_f-\frac{1}{2}\rho C_d A\,V^2-W_L \tag{16}$$

$$J_r\dot{\omega}_{wr}=-B_{wr}\omega_w^2-\mu_r W_r r_w+K_{Br}u_{Br} \tag{17}$$

$$J_f\dot{\omega}_{wf}=-B_{wf}\omega_w^2-\mu_f W_f r_w+K_{Bf}u_{Bf} \tag{18}$$

where W_r and W_f are obtained from Eqs. (2.a) and (2.b). We set the velocity of vehicle body equivalent to $V/r_w=x_1$, angular velocity of rear wheels as $\omega_r=x_2$, and angular velocity of front wheels as $\omega_f=x_3$. The state equations of braking deceleration are written as

$$\dot{x}_1=\frac{g\rho C_d A r_w\{l-(\mu_r-\mu_f)H\}}{2W\{l-(\mu_r-l_f)h\}}x_1^2+\frac{g(\mu_r l_f-\mu_f l_r)}{r_w\{l-(\mu_r-\mu_f)h\}}-\frac{glW_L}{r_w W\{l-(\mu_r-\mu_f)h\}} \tag{19}$$

$$\dot{x}_2=-\frac{B_{wr}}{J_r}x_2^2-\frac{3K_tK_e\eta i}{J_r(R_a+Ls)}x_2-\frac{\mu_r r_w^3\rho C_d A(H-h)}{2J_r\{l-(\mu_r-\mu_f)h\}}x_1^2+\frac{\mu_r r_w W l_f}{J_r\{l-(\mu_r-\mu_f)h\}}$$
$$+\frac{\mu_r r_w h W_L}{J_r\{l-(\mu_r-\mu_f)h\}}+\frac{K_B}{J_r}u_{Br} \tag{20}$$

$$\dot{x}_3=-\frac{B_{wf}}{J_f}x_3^2+\frac{\mu_f r_w^3\rho C_d A(H-h)}{2J_f\{l-(\mu_r-\mu_f)h\}}x_1^2+\frac{\mu_f r_w W(2h[\mu_r l_f-\mu_f l_r]-l_r l)}{J_f\{l-(\mu_r-\mu_f)h\}}$$
$$+\frac{\mu_f r_w h W_L}{J_f\{l-(\mu_r-\mu_f)h\}}+\frac{K_{BR}}{J_f}u_{Br} \tag{21}$$

As a result, we can get a state equation similar to Eq. (13).

$$\dot{x}=F(x)+Gu+Dw$$
$$y=x$$
$$x=[x_1\ x_2\ x_3]^T:\ u=[O\ u_{Br}\ u_{Bf}]^T$$

$$F=\begin{bmatrix} -\dfrac{g\rho C_d A r_w\{l-(\mu_r-\mu_f)H\}}{2W\{l-(\mu_r-\mu_f)h\}}x_1^2+\dfrac{g(\mu_r l_f-\mu_r l_f)}{r_w\{l-(\mu_r-\mu_f)h\}} \\ \left\{-\dfrac{B_{wr}}{J_r}x_2^2-\dfrac{3K_tK_e\eta i}{J_r(R_a+Ls)}x_2-\dfrac{\mu_r r_w^3\rho C_d A(H-h)}{2J_r\{l-(\mu_r-\mu_f)h\}}x_1^2-\dfrac{\mu_r r_w W l_f}{J_r\{l-(\mu_r-\mu_f)h\}}\right\} \\ \left\{-\dfrac{B_{wf}}{J_f}x_3^2+\dfrac{\mu_f r_w^3\rho C_d A l(H-h)}{2J_f\{l-(\mu_r-\mu_f)h\}}x_1^2+\dfrac{\mu_f r_w W\{2H(\mu_r l_f-\mu_f l_r)-l_r l\}}{J_f\{l-h(\mu_r-\mu_f)\}}\right\} \end{bmatrix}$$

$$G=\begin{bmatrix} a & 0 & 0 \\ O & \dfrac{K_{Br}}{J_r} & 0 \\ 0 & O & \dfrac{K_{Bf}}{J_f} \end{bmatrix};\ D=\begin{bmatrix} \dfrac{-gl}{r_w W\{l-(\mu_r-\mu_f)\}h} \\ \dfrac{\mu_r r_w h}{J_r\{l-(\mu_r-\mu_f)h\}} \\ \dfrac{\mu_r r_w h}{J_f\{l-(\mu_r-\mu_f)h\}} \end{bmatrix} \tag{22}$$

3. Control Logic : VSTC Theory

In general, we discuss a system of m inputs of n orders. The design algorithm comprises the following 3 steps.

Step 1 : Design of Sliding Surface

By considering space S of error vector e,

$$S=\{e:\ s(e,t)=0\}$$

$$s(e,t)=Ce(t)=0 \tag{23}$$

where $C\in R^{m\times n}$ is the weighting constant matrix, $e\in R^n$ and $s\in R^m$, $s(e,t)$ is the switching function which expresses the sliding surface. For simplicity, (e,t) is omitted in the following discussion.

$$e:\ (\text{real state})-(\text{reference state})=x-x_d \tag{24}$$

The state equation of e is derived from the following real state equation (25.a) and reference state equation (25.b).

$$\dot{x}=F(x)+G(x)u+Dw \tag{25.a}$$

$$\dot{x}_d=F(x_d)+G(x_d)u_d \tag{25.b}$$

$$\dot{e}=F(x)-F(x_d)+G(x)u-G(x_d)u_d+Dw$$

$$\dot{e}=F_e(e)+G_eu_e+Dw \tag{26}$$

In this work, we change the tracking control problem to the problem of designing a sliding surface of an error system which has $e=0$ as the origin, i.e., it become the problem of determining C. In general, it is very difficult to design a sliding surface for a nonlinear system. Thus, we propose an algorithm for designing the sliding surface of a simplified system equivalent to the original system. However, the condition that the two systems have the same sliding surface must be satisfied. The equivalent system is simpler than the original system regardless of whether the system is linear or nonlinear. Here, we linearize state equation (26) at equilibrium point $e=0$ and obtain the following equivalent system.

$$\dot{e}=Ae+Bu_e$$

$$A=\frac{\partial F_e(e)}{\partial e}\Big|_{e=0},\quad B=\frac{\partial G_e(e)}{\partial e}\Big|_{e=0} \tag{27}$$

Theorem[4] :

We consider system (26) and equivalent system (27). If there exist $\tilde{f}(e)$ and $\tilde{g}(e)$ which satisfy the matching conditions $F_e(e)-Ae=B\tilde{f}(e)$ and $G_e(e)-B=B\tilde{g}(e)$, then systems (26) and (27) will have the same sliding surface where B is a nonsingular matrix. If an equivalent system can be designed, we perform the following partition :

$$e=\begin{bmatrix}e_1\\ e_2\end{bmatrix},\quad C=[C_1\quad C_2],$$

$$A=\begin{bmatrix}A_{11} & A_{12}\\ A_{21} & A_{22}\end{bmatrix},\quad B=\begin{bmatrix}0\\ B_2\end{bmatrix},$$

where

$$e_1\in R^{n-m},\ e_2\in R^m,\ C_1\in R^{m\times(n-m)},\ C_2\in R^{(m\times m)}$$

$$A_{11}\in R^{(n-m)\times(n-m)},\ A_{12}\in R^{m\times m},\ A_{21}\in R^{m\times(n-m)}$$

From

$$\begin{bmatrix}e_1\\ s\end{bmatrix}=\begin{bmatrix}I & 0\\ C_1 & C_2\end{bmatrix}\begin{bmatrix}e_1\\ e_2\end{bmatrix}$$

we obtain the following result.

$$\dot{s}=[(C_1A_{11}-C_2A_{12})-(C_1A_{12}+C_2A_{22})C_2^{-1}C_1]e_1$$
$$+(C_1A_{12}+C_2A_{22})C_2^{-1}s+C_2B_2u_e$$

$$\dot{e}_1=(A_{11}-A_{12}C_2^{-1}C_1)e_1+A_{12}C_2^{-1}s \tag{28.a}$$

On the sliding surface, $s=0$ and the differential equation

$$\dot{e}_1=(A_{11}-A_{12}C_2^{-1}C_1)e_1 \tag{28.b}$$

describes the sliding mode. Now, from A_{11}, A_{12}, if we can select C_1, C_2 such that the real part of the eigenvalue of the matrix

$$K=(A_{11}-A_{12}C_2^{-1}C_1)$$

becomes $\lambda(K)<0$, the stability of the order-reduced sliding mode (Eq. (28.b)) is guaranteed. Then, we can obtain the switching function s

$$s=Ce=[C_1\quad C_2]e.$$

Step 2 : Design of Control Input

In reality, because of hysteresis, $s\neq 0$ and the ideal sliding mode can not occur. However, if the following condition is satisfied, a pseudo-sliding mode exists.

Existence condition of sliding mode[5] :

$$\lim_{s\to 0}s\,\dot{s}<0 \tag{29}$$

Reaching law[4] :

The above condition ensures the existence of the pseudo sliding mode and that the neigborhood of surface $s=0$ is reached. However, it does not clearly show either the finite duration or behavior of reaching dynamics. In this paper, we design a reaching control logic which guarantees existence condition (29) and clarifies the behavior of a general asymptotic convergence.

$$\dot{s}=-\beta\{f(s)+\psi\,\mathrm{sgn}(s)\} \tag{30}$$

where s is a switching function, $s=[s_1\ s_2\cdots s_m]^T$. β and ψ are any diagonal positive definite matrices. $\mathrm{sgn}(s)$ is the sign function.

$$\mathrm{sgn}(s)=[\mathrm{sgn}(s_1)\cdots\mathrm{sgn}(s_m)]^T$$

$$f(s)=[f_1(s_1)\cdots f_m(s_m)]^T$$

Functions $f_i(s_i)$ satisfy the following conditions.

$$s_if_i(s_i)>0;\ s_i\neq 0,\ i=1,\cdots,m$$

Equation (30) not only ascertains the reaching conditions, but also shows the dynamic behavior of reaching duration. $f(s)$ is any function designated by the designer. For example, setting $f(s)=s$, Eq. (30) will show the general sliding mode of $s=0$. A state trajectory which is off set from the sliding surface begins moving from the initial value $s=s(0)$ at $t=0$. After a finite period T, it will reach $s=0$.

$$T=\beta^{-1}\ln\left(1+\frac{|s(0)|}{\psi}\right) \tag{31}$$

From Eq. (30), we can ensure that the asymptotic sliding mode responds to all initial conditions of the

system. Then, from Eqs. (13), (23) and (30), u is obtained.

$$u=(CG)^{-1}\{C[-F-Dw+\dot{x}_d]-\beta C(x-x_d)+\beta\psi\cdot\mathrm{sgn}(s)\} \quad (32)$$

Step 3: Solution for Chattering Phenomenon

Because of $\mathrm{sgn}(s)$, u of Eq. (32) changes discontinously, and causes a chattering phenomenon. To solve this problem, we propose setting up, in so-called "ε aproximity" along sliding surface $s=0$, a saturated function. Consequently, u is smoothed as

$$u=(CG)^{-1}\left\{C[-F-Dw+\dot{x}_d]-\beta C(x-x_d)+\frac{\beta\psi}{\varepsilon}\cdot s\right\};\ |s|<\varepsilon \quad (33)$$

A diagram of the proposed algorithm is shown in Fig. 7.

Now, we consider the variation of parameters, and the error in modelling, and examine the robustness of the system. The robustness of control logic can be proven as follows.

Setting ΔF_e, ΔG_e and $\Delta D'$ as the variations of F_e, G_e, and D', system (26) becomes

$$\dot{e}=(F_e+\Delta F_e)+(G_e+\Delta G_e)u_e+D'w \quad (34)$$

We assume that $\Delta F_e'$ and $\Delta G_e'$ exist and satisfy the following matching conditions[4].

$$\Delta F_e=G_e\Delta F_e';\ \Delta G_e=G_e\Delta G_e';\ D'=G_e\Delta D'$$

$$C\dot{e}=C[F_e+\Delta F_e+(G_e+\Delta G_e)u_e+D'w]=0$$

From the above matching conditions,

$$C(F_e+G_e\Delta F_e'+G_e\Delta D'w)+CG_e(I+\Delta G_e')u_e=0$$

$$u_e=-(I+\Delta G_e')^{-1}(CG_e)^{-1}C[F_e+G_e\Delta F_e'+G_e\Delta D']$$

Substituting u_e into Eq. (34) gives

$$\dot{e}=F_e-G_e(CG_e)^{-1}CF_e.$$

As a result, it is apparent that tracking error e is not effected by ΔF_e and ΔG_e

4. Simulation and Considerations

We design a longitudinal control system for an electric vehicle using the above design algorithm. Its effectiveness is proven by simulation and a bench experiment. We consider the operation environments and comfortable ride when designing the running reference commmand velocity.

As a typical example, we consider the following reference command velocity.

Acceleration: $V(t)=V_0(1-e^{-mt})$ (35)

Constant velocity: $V(t)=V_0$ (36)

Deceleration: $V(t)=aTan(-bt+\mathrm{Tan}^{-1}c)$ (37)

$$A=\begin{bmatrix} -\dfrac{g\rho C_d A r_w(l-\mu_r H)x_{d1}}{W(l-\mu_r h)} & 0 \\ -\dfrac{\mu r_w^3\rho C_d A(H-h)x_{d1}}{J(l-\mu_r h)} & -\dfrac{2B_w x_{d2}+3K_t K_e\eta i}{J(R_a+Ls)} \end{bmatrix},$$

$$B=\begin{bmatrix} \alpha & 0 \\ 0 & \dfrac{3K\dot{K}_t\eta i}{J(R_a+Ls)} \end{bmatrix} \quad (38)$$

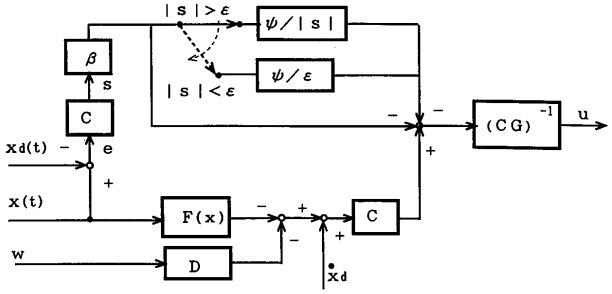

Fig. 7 Diagram of proposed VSTC control

Table 1 Inertial moment of mechanical components

PART NAMES	NOMINAL VALUE	ESTIMATED VALUE
MOTOR: ROTOR+FLYWHEEL + CLUTCH DISK Ie(kg.m2)	100	110
TRANSMISSION SYSTEM It(kg.m2)		
{ REDUCING GEAR: GEAR+		
RIGHT, LEFT SIDE FLANGE (kg.m2)	4550	4500
DRIVING PINION (kg.m2)	1058	1000
DRIVING SHAFT (kg.m2)	7066	7000
PROPELLER SHAFT } (kg.m2)	9731	10000
FINAL GEAR If(kg.m2)	47	50

Table 2 Parameters used in simulation

NOMINATION	EMPTY CAR	LOADED CAR
CAR BODY WEIGHT W (N)	12000	14500
HEIGHT OF CENTER OF GRAVITY h (m)	1	0.73
LONGITUDINAL POSITION OF CENTER OF GRAVITY lf(m)	1.62	1.8
WHEEL BASE l (m)	2.47	
TIRE RADIUS rw(m)	0.36	
AIR RESISTANCE COEF. Cd	0.28	0.3
EFFECTIVE SURFACE A (m2)	1.78	1.5
HEIGHT OF AIR RESISTANCE FORCE CENTER H (m)	1.2	1
TRANSMISSION GEAR		
1ST SPEED i1	3.4	
2ND SPEED i2	1.93	
3RD SPEED i3	3.9	
TRANSMISSION EFFECTIVE η	0.9	0.9
MOTOR TORQUE CONSTANT Kt(Nm/A)	0.75	0.75
REACTIVE ELECTROFORCE Ke	0.3	0.3
COIL RESISTANCE Ra(Ohms)	0.5	0.5
DISTURBANCE (Max) WL(N)	1000	1200
BRAKE COEFFICIENT Kbr, Kbf(N.m/V)	500	500

m is a positive constant which determines acceleration rate; a, b and c are calculated from Eq. (15.c) so that the vehicle body can be in decelerated stably and stopped within the shortest distance. Constants used in the simulation are shown in Tables 1 and 2. In the case of acceleration, in designing the sliding surface we assume that tracking error $e\ll x_d$, i.e., $x\approx x_d$. Linearizing system (26), we obtain the following results.

In this case, because of one input ($n=2$, $m=1$), there exists one sliding surface: $s=c_1e_1+c_2e_2$.

Similarly, in the case of deceleration,

$$A=\begin{bmatrix} -\dfrac{g\rho C_d A r_w\{l-(\mu_r-\mu_f)H\}}{2W(l-(\mu_r-\mu_f)h)}x_{d1} & 0 & 0 \\ -\dfrac{\mu_r r_w^3\rho C_d A(H-h)x_{d1}}{J_r\{l-(\mu_r-\mu_f)h\}} & -\dfrac{2B_{wr}(R_a+Ls)x_{d2}+3K_tK_e\eta i}{J_r(R_a+Ls)} & 0 \\ -\dfrac{\mu_f r_w^3\rho C_d A(H-h)x_{d1}}{J_f\{l-(\mu_r-\mu_f)h\}} & 0 & -\dfrac{2B_{wf}x_{d3}}{J_f} \end{bmatrix},$$

$$B=\begin{bmatrix} \alpha & 0 & 0 \\ 0 & \dfrac{K_{Br}}{J_r} & 0 \\ 0 & 0 & \dfrac{K_{Bf}}{J_f} \end{bmatrix} \tag{39}$$

Because of $n=3$ and $m=2$, two sliding surfaces exist.

$$C_1=\begin{bmatrix} c_1 \\ c_1' \end{bmatrix},\ C_2\begin{bmatrix} c_2 & c_3 \\ c_2' & c_3' \end{bmatrix}$$

$s_1=c_1e_1+c_2e_2+c_3e_3$, $s_2=c_1'e_1+c_2'e_2+c_3'e_3$

Corresponding to Eq. (28.b), A is changed depending upon x_d. However, because the conditions $l-\mu_r h>0$ and $l-\mu_r H>0$ are generally satisfied, and because A_{11} is negative and $A_{12}=0$, even if C_1 and C_2 are arbitrarily choosen, the system of Eq. (28.b) is stable, and the design of the sliding surface becomes simple. State trajectory starts from an arbitrary initial value and moves nearer to the sliding surface, either s_1 or s_2. Then it slides along this surface to the line of intersection L between s_1 and s_2, and converges along this line to the origin ($e=0$). This behavior is shown in Fig. 8.

Line L is the solution of the following simultaneous equations.

$s_1=c_1e_1+c_2e_2+c_3e_3=0$

$s_2=c_1'e_1+c_2'e_2+c_3'e_3=0$

$$L=\begin{cases}(c_1c_3'-c_1'c_3)e_1+(c_2c_3'-c_2'c_3)e_2=0\\(c_1c_2'-c_1'c_2)e_1+(c_3c_2'-c_3'c_2)e_3=0\end{cases}$$

In this simulation, sliding line s, sliding surfaces s_1 and s_2, and line L are set up as follows.

$s_1=0.5e_1-5e_2-0.5e_3=0$;

$s_2=-120e_1+5e_2-0.5e_3=0$

$$L=\begin{cases}-57.5e_1-60e_2=0\\-597.5e_1+5e_3=0\end{cases};\ s=0.5e_1+0.1e_2=0$$

For the existence of disturbance, the result of tracking reference command velocity $V=100$ km/h is shown in Fig. 9. In spite of the existence of disturbance, operation is nearly stable and the system is proven to have superior dynamic response and robust stability.

Because the inertia of the vehicle body is large, chattering cannot be found in its tracking velocity, but chattering obviously occurs in control input u. On the contrary, in Fig. 10, the saturated function is used, and its effectiveness in alleviating chattering is shown. In acceleration, control voltage is indicated as positive, and in deceleration, it is shown as a negative value.

Figures 11(a) and (b) show the variation of rolling friction during running. Initially, because the

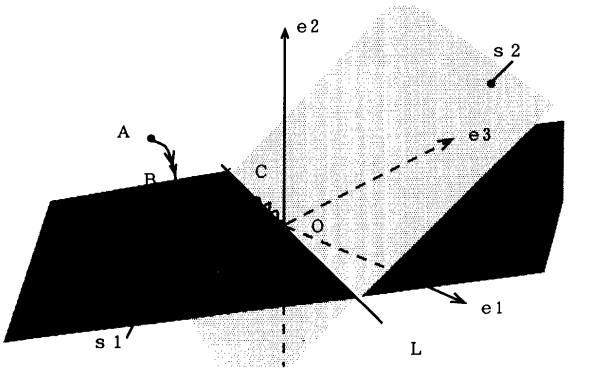

Fig. 8 The behavior of state trajectory

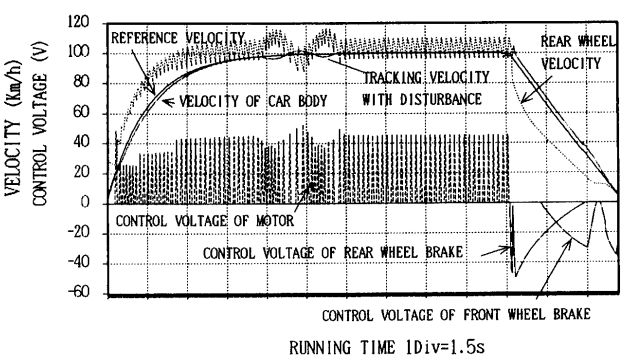

Fig. 9 Tracking velocity and chattering phenomenon $\varepsilon=0$; $\beta=8$; $\psi=1$

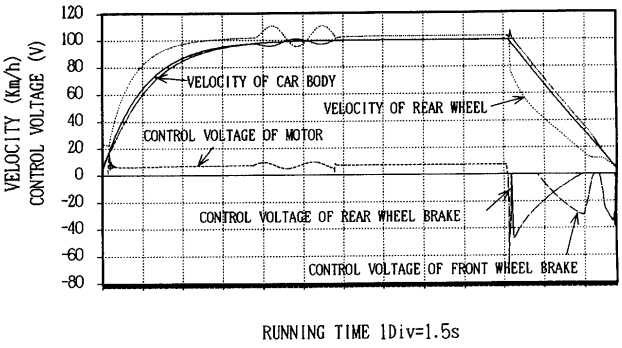

Fig. 10 Tracking velocity and the alleviation of chattering, $\varepsilon=2$; $\beta=8$; $\psi=1$

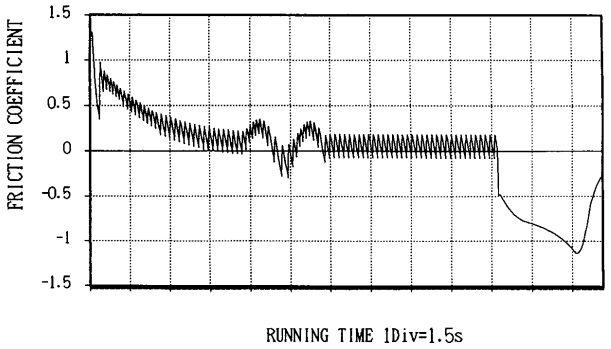

Fig. 11(a) Rolling friction coefficient of rear wheels and chattering phenomenon, $\varepsilon=0$; $\beta=8$; $\psi=1$

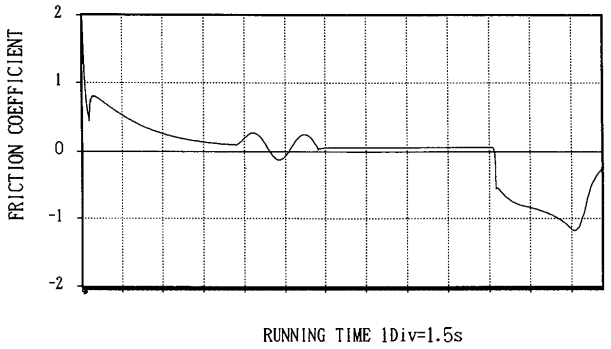

Fig. 11(b) Rolling friction coefficient and chattering phenomenon with $\varepsilon=0$; $\beta=8$; $\psi=1$

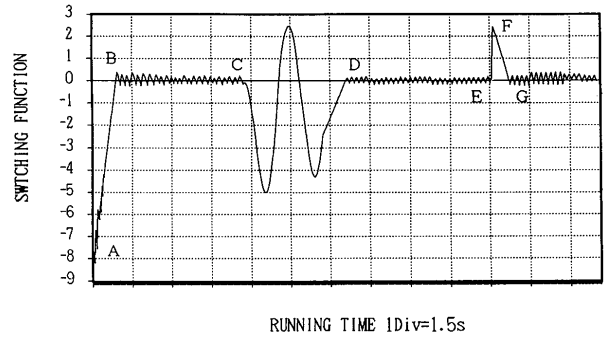

Fig. 12 Switching function s and chattering phenomenon with $\varepsilon=0$; $\beta=8$; $\psi=1$

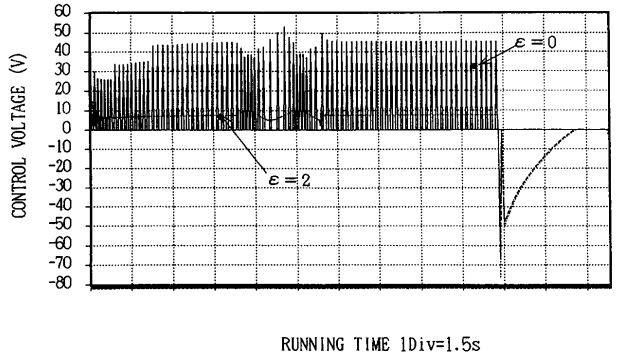

Fig. 13 Control voltage against variation of control parameter ε; $\varepsilon=0, 2$; $\beta=8$; $\psi=1$

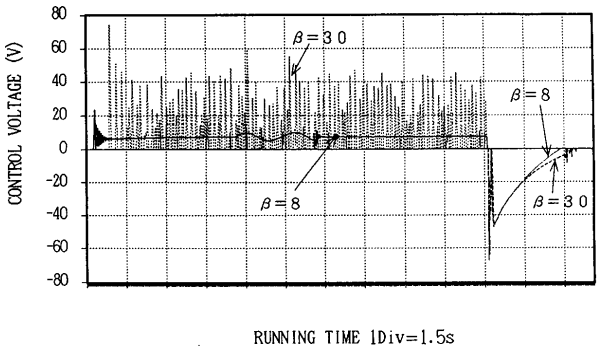

Fig. 14 Control voltage against variaton of control parameter β; $\beta=8, 30$; $\varepsilon=2$; $\psi=1$

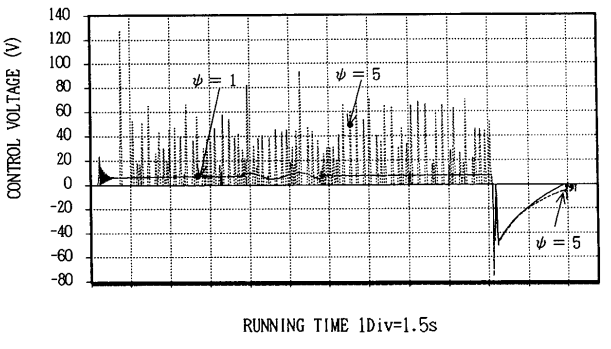

Fig. 15 Control voltage against variation of ψ $\psi=1, 5$; $\varepsilon=2$; $\beta=8$

difference between the velocity of the wheel tire and the velocity of the vehicle body is large, slip ratio and friction resistance are also large. However, in the constant velocity period, this difference becomes small, thus friction resistance also decreases.

In the constant velocity period, because air resistance and viscous resistance do not change, control input and friction resistance are invariable.

Figure 12 shows the variation of switching function s. s switches around zero. At the initially start (A B), when disturbance occurs (C D) or when the running condition is changed from constant velocity to deceleration (E F G), the siding mode disappears, but it quickly returns to a steady stable state.

Figure 13 shows the variation of control voltage against the variation of ε. ε is the factor governing the thickness of the boundary layer which alleviates the chattering phenomenon. When the value of ε is large, the width of the region alleviating chattering increases, but dynamic response and robustness deteriorate. When ε is small, high tracking accuracy is obtained, but chattering becomes violent. In particular when $\varepsilon=0$, the alleviation effect is lost completely and chattering is the most violent.

Figure 14 shows the variation of control voltage against parameter β. β is the factor determing the convergent speed of tracking error. If its value

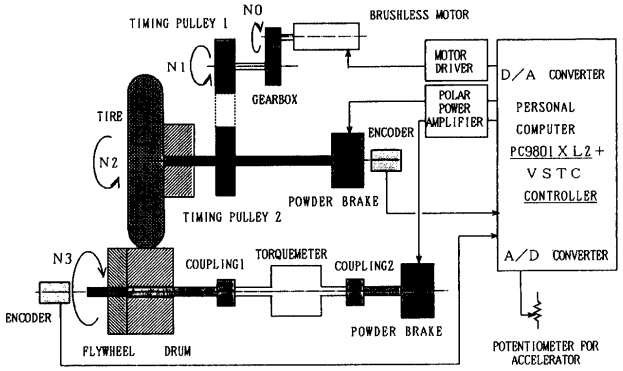

Fig. 16 Structure of experiment apparatus

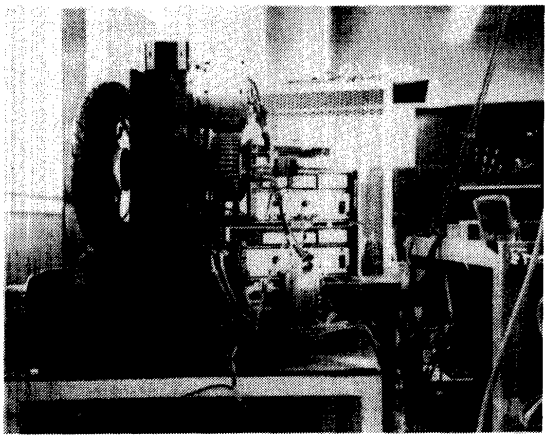

Fig. 17 Experimental apparatus

increases, convergence becomes faster, but chattering occurs easily. Figure 15 shows the variation of control voltage against parameter ϕ. Parameter ϕ indicates the effects of variable structure, and ensures disturbance rejection and robustness of the system.

To examine the effectiveness of control logic in application, we carried out the bench experiment on the "ONE WHEEL MODEL", as shown in Figs. 16 and 17. A typical experimental result is shown in Fig. 18.

5. Conclusion

In this paper, we discussed the algorithm for longitudinal control of an electric vehicle driven with

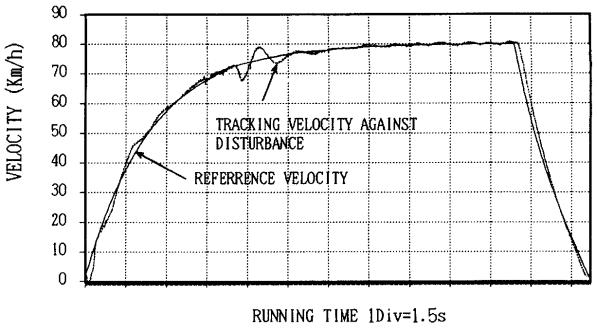

Fig. 18 Experimental tracking result

a brushless motor, based on VSTC control. Regardless of it being a nonlinear control system, with this control algorithm, the design is simple, the level of robustness is high and the algorithm is effective against disturbance and uncertainty of modelling.

Moreover, because it can effectively remove chattering, it is expected to play an important role in practical applications.

Futhermore, with longitudinal control of an electric vehicle, it provides a comfortable ride. Treating the electric vehicle as a nonlinear control system, due to the effect of VSTC, with only simple input, we can achieve accurate tracking to command velocity.

References

(1) Dote, Y. and Kinoshita, S., Basic and Application of Brushless Servo Motor (1985), p. 100, Sogo Denshi Publisher Corp.

(2) Automobile Technology Society, Automobile Technology Handbook, (1959), 2-2-13, Tosho Publisher Corp.

(3) Salman, M. A., Robust Servo-Electronic Control for Brake Force Distribution, Trans., of the ASME, J. Dyn. Syst. Meas. and Control, 12 (1990), p. 442.

(4) Gao, W. B. and Hung, J. C., Variable Structure Control of Nonlinear Systems: A New Aproach, IEEE Trans. Ind Electron., Vol. 40, No. 1 (1993), p. 45.

(5) Utkin, V. I., Variable Structure Systems with Sliding Modes, IEEE Trans. on Automatic Control., Vol. 22, No. 2 (1977), p. 212.